CrystEngComm

Accepted Manuscript

ROYAL SOCIETY OF CHEMISTRY

www.rsc.org/crystengcomm

Facile synthesis of β-$NaGdF_4$:Yb/Er@CaF_2 nanoparticles with enhanced upconversion fluorescence and stability via a sequential growth process

Bin-Bin Ding, [a] Kun Liu, [a] Fu Zhang, [a] Yang Wang, [b] Sheng Cheng, [b] Yang Lu,*, [c] Hai-Sheng Qian *,[a]

[a]*Department of Medical Materials and Rehabilitation Engineering, School of Medical Engineering, Hefei University of Technology, Hefei 230009, P. R. China.*

[b]*Analytical and Testing Center, Hefei University of Technology, Hefei 230009, P. R. China.*

[c]*Department of Chemistry, Hefei University of Technology, Hefei 230009, P. R. China.*

RECEIVED DATE (to be automatically inserted after your manuscript is accepted if required according to the journal that you are submitting your paper to)

Corresponding author. Fax: 0086 551 62901285, Fax: 0086 551 62901285. E-mail: yanglu@hfut.edu.cn (Y. Lu); shqian@hfut.edu.cn (H. S. Qian)

Abstract

Upconversion fluorescent nanostructures with controlled size and morphologies have been attracted much attention owing to their potential and important applications in bioimaging, photodynamic therapy, solar cell and so on. In this work, we describe a facile successive process to fabricate β-$NaGdF_4$:Yb,Er nanocrystals coated with ultrathin layer of CaF_2 with enhanced upconversion fluorescence and stability. The as-prepared β-$NaGdF_4$:Yb,Er@CaF_2 nanoparticles were investigated by X-ray diffraction (XRD), transmission electron microscopy (TEM, JEM 21000), fluorescence spectrometer (Hitachi High-Technology Corporation, F-2700) and inductively coupled plasma atomic emission spectrometry (ICP-AES); respectively. The as-prepared core-shell nanoparticles show enhanced upconversion fluorescence and superior magnetic resonance (MR) relaxivity. In addition, the as-prepared β-$NaGdF_4$:Yb,Er@CaF_2 nanoparticles show enhanced chemical stability after surface functionalization and transferred into the aqueous solution.

Key words: Upconversion, Core-shell Nanostructures, CaF_2, Hexagonal Phase, Facile synthesis, Stability

1. Introduction

Core-shell nanostructures with improved chemical and physical properties have attracted much attention for the past two decades.[1,2] Lanthanide ions doped upconversion nanoparticles (UCNPs), unique and attractive type of phosphors, which have been extensively studied.[3-6] Compared to down-conversion fluorescent materials, UC fluorescent NPs have several significant advantages: such as low toxicity,[7] low autofluorescence background,[8] reduced photo-bleaching and blinking,[9] and low photodamage to living organisms and high light excitation penetration depth in biological tissues.[10] Up to date, a variety of techniques have been developed to synthesize UC nanomaterials with well controlled size, shape and nanostructures owing to the potential applications in bioimaging,[11-14] photodynamic therapy,[15,16] solar cell,[17] and so on. In recent years, special efforts have been paid to synthesize lanthanide ions doped upconversion core-shell nanostructures with enhanced physical property and multi-functionalities including $NaYF_4$:Yb/Er@$NaGdF_4$,[18] $NaYF_4$:Yb/Tm@$NaYF_4$:Yb/Er,[19] $NaYbF_4$:Er/Tm@$NaGdF_4$,[20] β-$NaYF_4$:Nd,Yb,Er(Tm)@$NaYF_4$:Nd,[21] $NaGdF_4$:Yb,Tm@$NaGdF_4$:Dy(Sm, Eu, Tb)@$NaYF_4$,[22] and so on. These nanostructures are of scientific importance to widely application in specific targeting, multimodal imaging and therapeutic delivery.

However, it has attracted much attention that the biological safety caused by the leaking of the rare earth ions.[23,24] In contrast to other protection layers, CaF_2 has its unique advantages owing to its better chemical stability, biocompatibility and good optical transparency.[25-27] In particular, CaF_2 crystals with low lattice mismatch with $NaReF_4$ nanocrystals. Therefore, CaF_2 shell can protect the rare-earth ions from leaking to enhance the chemical stability and physical properties via epitaxial growth of a thin layer of CaF_2 on the surface of UCNPs. So far, much effort has been made to synthesize RE^{3+}-doped CaF_2 or UCNPs@CaF_2 nanocrystals via different methods. Recently, Prof. Li and his co-workers developed a facile wet chemical technology to prepared monodispersed CaF_2:Yb^{3+}/Er^{3+} nanocrystals.[25] Ln^{3+}-doped or Ln^{3+} and Mn^{2+}-co-doped hollow CaF_2 was successfully fabricated by Lin group for

multimodal bioimaging.[28-29] More recently, Han and co-workers reported a novel (α-$NaYbF_4$:Tm^{3+})/CaF_2 nanoparticles; which exhibited highly efficient NIR_{in} -NIR_{out} upconversion via co-thermolysis of $Na(CF_3COO)$, $RE(CF_3COO)_3$ and $Ca(CF_3COO)_2$ in oleic acid/1-octadecene.[26-27] Chen group prepared monodisperse and sub-10 nm lanthanide-doped CaF_2 nanostructures.[30] Yan group reported α-$NaGdF_4$:Yb,Er@CaF_2 NPs with 10 nm in diameter by co-thermolysis approach.[31]

Yb^{3+} and Er^{3+} co-doped $NaGdF_4$, a superior UC luminescent material, as dual-modal contrast agents, could simultaneously achieve UC fluorescent imaging and magnetic resonance imaging because of magnetism of Gd^{3+} ions.[32-35] Up to date, there are few reports about fabrication of the hexagonal $NaGdF_4$:Yb/Er@CaF_2 core-shell nanoparticles. Herein, β-$NaGdF_4$:Yb/Er@CaF_2 nanoparticles have been synthesized via a modified sequential growth process.[16] At first, β-$NaGdF_4$:Yb/Er nanocrystals with *ca.* 12 nm in diameter were achieved by quick injection of the rare earth ions ($Gd_{0.78}Yb_{0.2}Er_{0.02}$)-oleate precursor solution into a high boiling-point hot solvent containing NH_4F and NaOH. Calcium oleate solution prepared from calcium oxides and oleic acid was injected into the previous solution containing pre-synthesized β-$NaGdF_4$:Yb/Er nanocrystals to epitaxially grow a thin layer of CaF_2 to form β-$NaGdF_4$:Yb/Er@CaF_2 nanoparticles, as illustrated in Fig. 1a. In this work, amounts of NaOH and NH_4F play important role in formation of this kind of core-shell nanoparticles. The upconversion fluorescence, magnetic resonance (MR) relaxivity and chemical ability were also investigated.

2. Experimental

2.1 Reagents

Sodium hydroxide (NaOH), ammonium fluoride (NH_4F), calcium oxide (CaO, 99%), $GdCl_3·6H_2O$ (99.99%), $YbCl_3·6H_2O$ (99.99%) and $ErCl_3·6H_2O$ (99.99%) were purchased from Aladdin Chemical Reagent Corporation. Oleic acid (OA, 90%) was purchased from Sigma-Aldrich Chemical Reagent Corporation. Octadecene (ODE, 90%) was purchased from Acros Organics Chemical Reagent Corporation. Methanol (CH_3OH) was purchased from Sinopharm Chemical Reagent Corporation,

China. All the chemical reagents were used as received and without further purification.

2.2 Synthesis of Gd/Yb/Er-oleic and Ca-oleic complex. 0.195 mmol $GdCl_3$, 0.05 mmol $YbCl_3$, 0.005 mmol $ErCl_3$ and OA (3 mL) were added into a 50 mL three-neck flask and heated to 120 ^oC for 30 min to form clear solution (Ln-OA complex). Ca-oleic complex was synthesized from CaO (0.25 mmol) and OA (3 mL) at 150 ^oC for 30 min. The Gd/Yb/Er-oleic (Ln-OA) and Ca-oleic (Ca-OA) complex solution were stable and used as stock solution.

2.3 Synthesis of β-$NaGdF_4$:Yb/Er@CaF_2 core-shell NPs with different shell thickness. In a typical protocol, OA (6 mL) and ODE (15 mL) were added into a three-neck reaction flask with magnetic stirring, and 10 mL methanol solution containing NH_4F (0.0741 g) and NaOH (0.0500 g) was added into the flask. Thereafter, the solution was slowly heated to evaporate methanol, maintained at 100 ^oC for 10 min, degassed at 100 ^oC for 10 min, and then heated to 280 ^oC under argon. Subsequently, the Ln-OA complex (0.25 mmol was quickly injected into the reaction vessel and maintained at 280 ^oC for 40 min. Then, the Ca-OA complex was slowly injected and the solution was maintained for 30 min. After the solution was cooled down naturally, the product was precipitated using ethanol and washed with ethanol/water (1:1 v/v) for three times. Finally, the $NaGdF_4$:Yb/Er@CaF_2 NPs were stocked and dispersed in cyclohexane. The synthetic procedure of $NaGdF_4$:Yb/Er@CaF_2 NPs of different shell thickness was same as that synthesized the above-mentioned NPs, except that Ca (0.125 mmol)-OA complex was injected.

2.4 Surface functionalization of β-$NaGdF_4$:Yb/Er@CaF_2 core-shell nanoparticles.

Hydrophobic β-$NaGdF_4$:Yb/Er@CaF_2 nanoparticles could be easily converted into hydrophilic ones using polyacrylic acid (PAA, Mn = 2000) coating by a modified ligand exchange procedure.[36-41] In a typical process, a mixing solution of 1 mL 0.05 M β-$NaGdF_4$:Yb/Er@CaF_2 nanocrystals solution in cyclohexane, 50 mg PAA and 16 mL ethylene glycol were loaded in a 50 mL three-neck reaction flask and was vigorously stirred for 10 min. Then, the solution was slowly heated to 80 ^oC and maintained for 1.5 h to evaporate cyclohexane. After the solution was cooled naturally, the UCNPs@PAA

nanoparticles were collected by centrifugation and washed with ethanol and water for three times; respectively. The hydrophilic β-$NaGdF_4$:Yb/Er@CaF_2 nanoparticles aqueous solution was dispersed using 10 mL double-distilled water.

In order to determine the concentration of Gd^{3+} delivered from the nanoparticles, the clear solution 100 μL was collected from the β-$NaGdF_4$:Yb/Er@CaF_2 nanoparticles aqueous solution at 24 h intervals and analyzed using inductively coupled plasma atomic emission spectrometry (ICP-AES). For comparison, β-$NaGdF_4$:Yb/Er core nanocrystals was modified via the same process.

2.5 Characterization

The phase of the as-prepared product was characterized by X-ray power diffraction (XRD) analyses; which was carried out on a Philips X'Pert PRO SUPER X-ray diffractometer equipped with graphite monochromatized Cu Kα radiation and the operation voltage and current were maintained at 40 kV and 40 mA; respectively. The morphology and size of the samples were investigated by transmission electron microscopy (TEM, JEM 21000). Samples were prepared by placing a drop of dilute dispersions in cyclohexane on the surface of a copper grid. Upconversion fluorescent spectra were measured on an F-2700 fluorescence spectrometer (Hitachi High-Technology Corporation), where an external CW laser at 980 nm replaced the Xenon lamp as the excitation source. Inductively coupled plasma atomic emission spectrometry (ICP-AES) was employed to determine the concentration of Gd^{3+} in the solutions. The relaxivity measurements were carried out on a 3 T clinical MRI instrument (GE Signa 3.0 T HD, Milwaukee, WI, USA). A series of aqueous solutions with different concentrations of $NaGdF_4$:Yb,Er@CaF_2@PAA and Gd-DTPA particles were prepared and transferred into 1.5 mL Eppendorf tubes for longitudinal magnetic relaxivity measurements.

3. Results and discussion

The morphology and size of the as-prepared $NaGdF_4$:Yb/Er@CaF_2 nanoparticles obtained from 0.05g NaOH (1.25 mmol), 0.0741 g NH_4F (2 mmol), 0.25 mmol $Gd_{0.78}Yb_{0.2}E_{r0.02}$-oleate and 0.25 mmol Ca-oleate were investigated by transmission electron microscopy and field-emission scanning electron

microscopy; respectively. Fig. 1b shows the TEM images of $NaGdF_4$:Yb/Er nanoparticles with sphere-like and 12 nm in diameter. After growing a CaF_2 shell, monodisperse nanocrystals with an average size of 13.3 nm (the distance of opposite sides of regular hexagon), larger than that of the core nanocrystals, were obtained, suggesting that CaF_2 nanocrystals with about 1 nm in shell width were grown on the surface of $NaGdF_4$:Yb/Er nanocrystals, as shown in Fig. 1c, d. Fig. 1e show the HRTEM image of a single hexagonal nanocrystal; in which a lattice distance of 0.52 nm in the inner region corresponding to the d spacing of the (100) or (010) lattice planes of the $NaGdF_4$:Yb/Er. In addition, the lattice distance near to the surface of 0.56 nm, larger than that's of inner's; which is in good agreement with the (100) lattice planes of CaF_2. The formation of hexagonal core-shell nanoparticles probably be attributed to the low lattice mismatch for the (100) crystal planes between CaF_2 and $NaGdF_4$. The XRD pattern of the as-synthesized $NaGdF_4$:Yb/Er@CaF_2 NPs has been characterized and shown in Fig. S1 (in the ESI) and all the strong diffraction peaks can be indexed to pure hexagonal phase of $NaGdF_4$; which is in good agreement with the literature values (JCPDS no. 27-0699). The characterization peaks for CaF_2 was not observed; which is similar to the previous works.[42,43] Chemical compositions of the β-$NaGdF_4$:Yb/Er@CaF_2 nanoparticles were also characterized by energy-dispersive X-ray analysis (EDX) (Fig. S2, in the ESI), in which the Ca element is approximately *ca.* 6 at%, calculated according to the data on atomic percentages and the detailed elemental compositions were listed in Table S1 (in the ESI). Elemental mapping of Na, F, Gd, Yb, Ca and Er in the NPs for the as-prepared β-$NaGdF_4$:Yb,Er@CaF_2 core/shell NPs was shown in Fig. S3 (in the ESI), which provides evidence of the presence of the elements of Gd, Yb, Er, F and Ca; the merged elemental mapping picture suggesting the β-$NaGdF_4$:Yb/Er@CaF_2 core/shell NPs achieved successfully.

In addition, the shell width for CaF_2 shell can be tunable via adjusting the amount of Ca-oleate precursor. Fig. S4a, b (in the ESI) show the transmission electron microscopy images of the core $NaGdF_4$:Yb/Er NPs before inject of 0.125 mmol Ca-oleate precursor and $NaGdF_4$:Yb/Er@CaF_2 nanoparticles. The $NaGdF_4$:Yb/Er nanoparticles are with similar size; which is in agreement with

previous experiments. The $NaGdF_4$:Yb/Er@CaF_2 nanoparticles are with average size of 12.6 nm in diameter via statistical analysis (Fig. S4e, in the ESI). By comparing single core and core-shell thickness, it is clear that shell thickness is very thin, only about 0.5~0.6 nm. The HRTEM images of the nanocrystals show a lattice distance of 0.52 nm for the d spacing of the (100) lattice planes of the $NaGdF_4$:Yb/Er (Fig. S4g, in the ESI). Both the core (bright) and the shell (dark) in dark-field scanning transmission electron microscopy images of the core-shell $NaGdF_4$:Yb/Er@CaF_2 NPs are clearly visible; which displays a successful epitaxial growth of CaF_2 shells on the $NaGdF_4$:Yb/Er again, as shown in Fig. S4h,i (in the ESI).

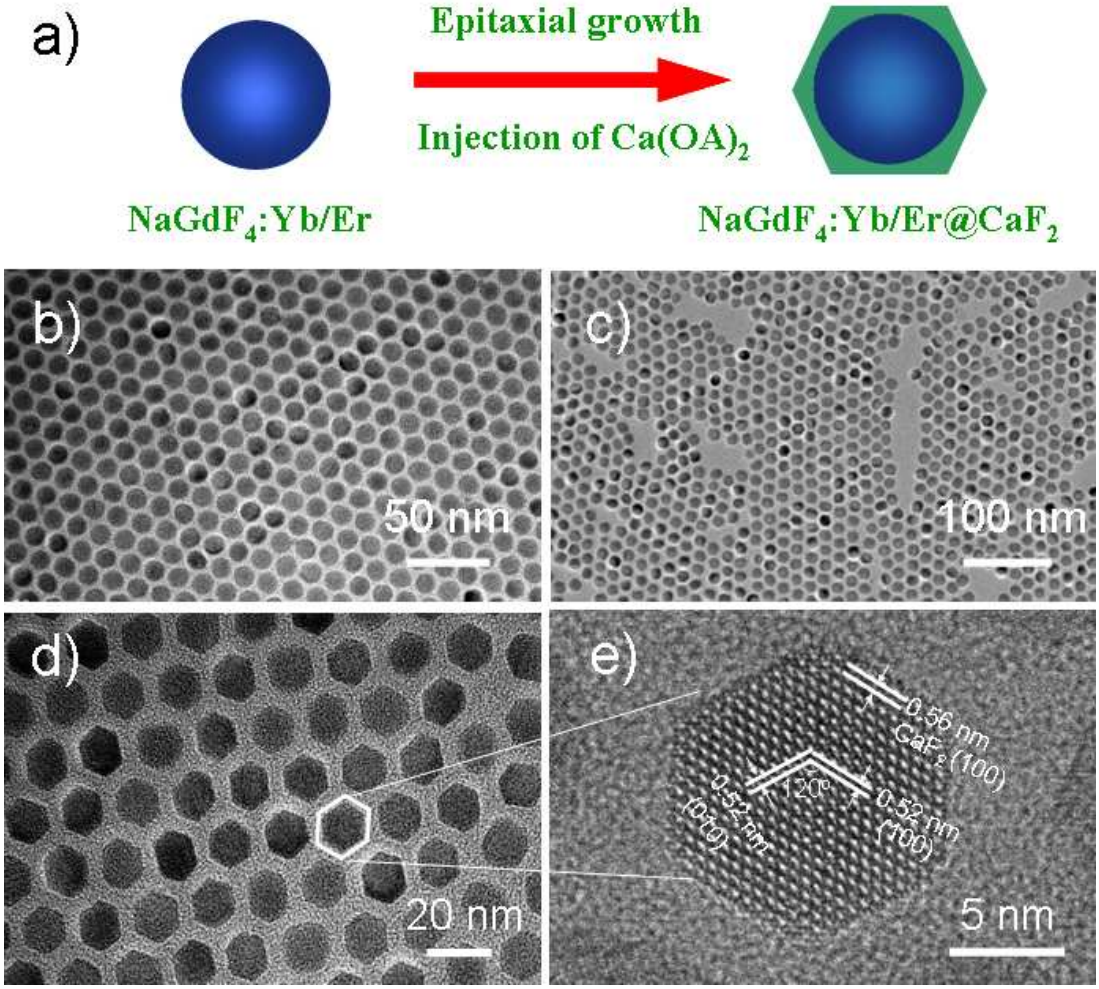

Fig. 1. Successful epitaxial growth of CaF_2 shells on $NaGdF_4$:Yb/Er core NPs, resulting in uniform and monodispersed $NaGdF_4$:Yb/Er@CaF_2 core/shell NPs. (a) Schematic illustration of the epitaxial growth of CaF_2 shells on $NaGdF_4$:Yb/Er core NPs; (b) transmission electron microscopy (TEM) images of $NaGdF_4$:Yb/Er core nanocrystals synthesized from 0.05 g NaOH (1.25 mmol), 0.0741 g NH_4F (2 mmol), 0.25 mmol $Gd_{0.78}Yb_{0.2}Er_{0.02}$-oleate at 280 ^oC; (c, d) TEM of $NaGdF_4$:Yb/Er@CaF_2 core-shell NPs obtained from 0.05 g NaOH (1.25 mmol), 0.0741 g NH_4F (2 mmol) and 0.25 mmol $Gd_{0.78}Yb_{0.2}Er_{0.02}$-oleate and 0.25 mmol Ca-oleate at 280 ^oC; (e) high resolution transmission electron microscopy (HRTEM) images of a hexagonal nanoparticle.

In this letter, amount of NaOH plays important role in coating of the ultrathin layer of CaF_2 layer on the $NaGdF_4$:Yb/Er to form core-shell nanoparticles. In this process, excessive F^- reactants exist as NaF because of equal mole for NaOH and NH_4F after $NaGdF_4$:Yb/Er nanoparticles achieved. If the amount of NaOH was decreased to 0.02 g, small nanoparticles of CaF_2 with ca. 2-3 nm in diameter are clearly observed when other synthetic condition was kept at same (Fig. S5a, in the ESI), which is ascribed to the rapid reaction for excessive NH_4F (HF) and Ca-oleate. As shown in Fig. S5b (in the ESI), when the amount of NaOH was increased to 0.16 g, small nanoparticles of CaF_2 with several nanometers in diameter was also appeared, which may be from the conversion of pre-synthesized $Ca(OH)_2$. For comparison, the as-prepared $NaGdF_4$ nanoparticles were obtained from 0.05 g NaOH (1.25 mmol), 0.0741 g NH_4F (2 mmol) and 0.25 mmol $Gd_{0.78}Yb_{0.2}Er_{0.02}$-oleate via the similar protocol for the $NaGdF_4$:Yb/Er@CaF_2 core/shell NPs, when 3 mL oleic acid was injected in place of Ca-oleate solution and the other condition was kept at same. The TEM image shows that the $NaGdF_4$:Yb/Er nanoparticles are sphere-liked with similar size, as shown in Fig. S6 (in the ESI).

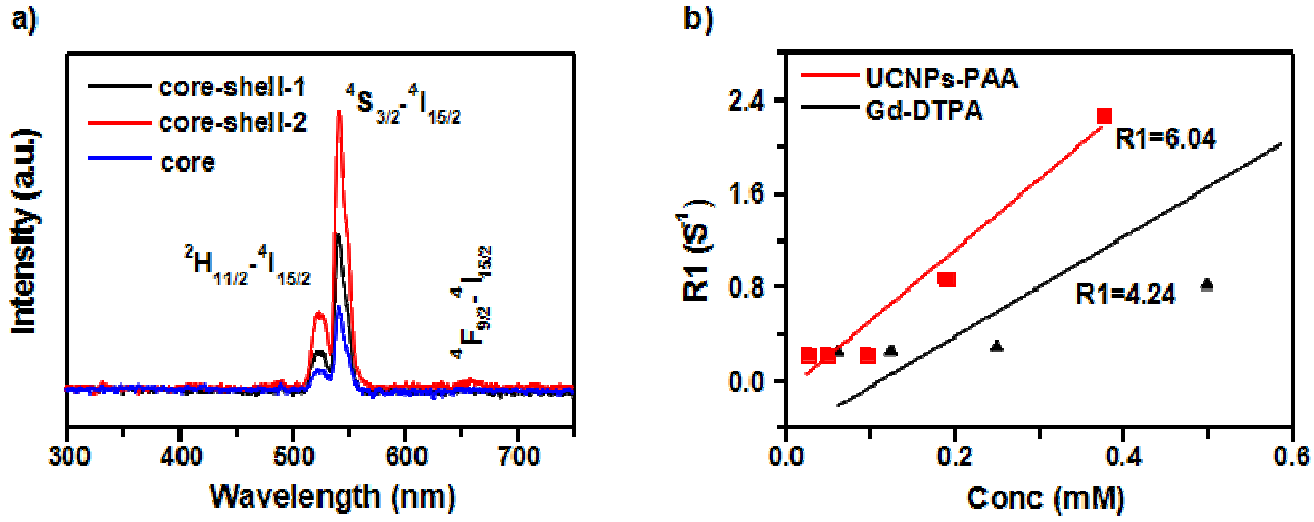

Fig. 2. (a) The comparison of UC emissions of β-$NaGdF_4$:Yb/Er (20/2 mol%) (core) NPs, β-$NaGdF_4$:Yb/Er (20/2 mol%)@CaF_2 (OA-Ca=0.125 mmol, denoted as core-shell-1) NPs and β-$NaGdF_4$:Yb,Er (20/2 mol%)@CaF_2 (OA-Ca=0.25 mmol, denoted as core-shell-2) NPs upon excitation at 3 w of 980 CW laser under the identical experimental conditions. (b) The comparison of longitudinal relaxivity R1 of the surface-modified β-$NaGdF_4$:Yb/Er@CaF_2 NPs (red) and Gd-DTPA (black).

In this work, the as-prepared Yb and Er ions doped $NaGdF_4$ nanoparticles show good upconversion fluorescence. Fig. 2a shows that the luminescent emission spectra of the β-$NaGdF_4$:Yb/Er (20/2 mol%) core and the β-$NaGdF_4$:Yb/Er(20/2 mol%)@CaF_2 core/shell NPs dispersed in cyclohexane excited using 980 nm laser. The UC fluorescence peaks located at 520, 540 and 656 nm; which was assigned to the transitions from $^2H_{11/2}$, $^4S_{3/2}$, and $^4F_{9/2}$ to $^4I_{15/2}$ of Er; respectively.[44] The UC luminescent intensity for the core-shell nanoparticles obtained from 0.25 mmol Ca-oleate was enhanced (2-3 folds), illustrating the formation of β-$NaGdF_4$:Yb,Er@CaF_2 core-shell nanostructures. In a word, the β-$NaGdF_4$:Yb,Er@CaF_2 core-shell NPs have been fabricated successfully via this sequential synthetic route. These β-$NaGdF_4$:Yb,Er@CaF_2 nanoparticles can serve as T1 contrast agent. As we well know that paramagnetic Gd^{3+} ion-based materials including Gd^{3+} ions and chelating ligands are T_1 (positive) contrast agents. Previous study revealed that Gd-DTPA (Magnevist), a kind of commonly used contrast agent is with longitudinal relaxivity (R1 = 3.7 $mM^{-1}s^{-1}$) and transverse relaxivity (R2 = 5.8 $mM^{-1}s^{-1}$).[45] Fig. 2b shows the MR relaxivity of the nanocrystals dispersed in water, which are calculated from a fitting curve of the longitudinal relaxation rate (1/T1, R1) as a function of the Gd^{3+} concentration (Fig. 2b). For comparison, commonly used contrast agents such as Gd-DTPA (Magnevist) were used in similar condition. The longitudinal relaxivity (R1) for the core-shell nanoparticles is calculated to 6.04 $mM^{-1}s^{-1}$, which is higher than that of Gd-DTPA (4.24 $mM^{-1}s^{-1}$). The MR longitudinal relaxivity data are impressive, which demonstrates that the as-prepared β-$NaGdF_4$:Yb,Er@CaF_2 nanoparticles are promising candidate as T1 contrast agent.

Obviously, the shell layer of CaF_2 could prevent partly the leakage of Gd^{3+} ions according to previous study.[46] Inductively coupled plasma atomic emission spectrometry (ICP-AES) was also employed to determine the concentration of Gd^{3+} in the solutions. Fig. 3 shows that 0.2 % Gd ions for the β-$NaGdF_4$:Yb,Er@CaF_2 core-shell nanoparticles were released lower than that of the β-$NaGdF_4$:Yb,Er core nanocrystals when the concentration of the β-$NaGdF_4$:Yb,Er nanoparticles and β-$NaGdF_4$:Yb,Er@CaF_2 nanoparticles was kept at the same. Therefore, in this work, β-

$NaGdF_4$:Yb,Er@CaF_2 core-shell nanoparticles with enhanced upconversion fluorescence and chemical stability have been achieved via a sequential growth process; which are promising candidate as T1 contrast agent and used as multimodal bioimaging agents.

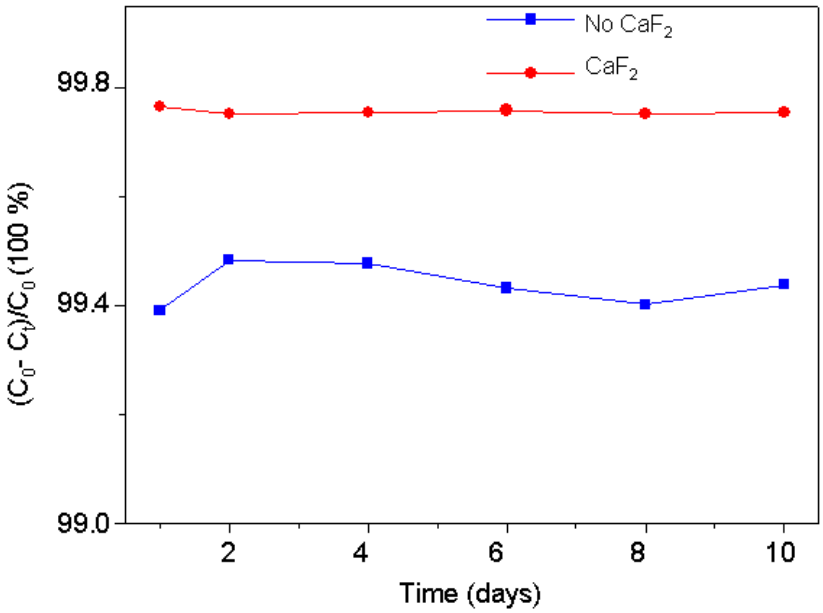

Fig. 3. ICP-AES analysis results: red line and black line represent the Gd^{3+} ion concentrations not released from CaF_2-shelled and no CaF_2-shelled NPs, respectively. C_0 and C_T are concentration of Gd^{3+} ions in the original solution and released in the solution for different time (T), respectively.

4. Conclusions

In summary, β-$NaGdF_4$:Yb/Er coated with ultrathin layer of CaF_2 core-shell nanoparticles have been synthesized successfully via a facile sequential growth process; which are mainly composed of hexagons of *ca.* 13 nm per side. 2-3 folds enhancement in the fluorescence intensity was also observed for the emission peaks corresponding to the transitions of $^2H_{11/2}$, $^4S_{3/2}$, and $^4F_{9/2}$ to $^4I_{15/2}$ of Er. Additionally, the shell CaF_2 layer decreases surface defects; which not only increases luminescent intensities, but also improves the biocompatibility and stability of nanoparticles and prevents the leakage of RE^{3+} ions. The longitudinal relaxivity (R1) for the core-shell nanoparticles is calculated to 6.04 $mM^{-1}s^{-1}$; which is higher than that of Gd-DTPA (Magnevist, 4.24 $mM^{-1}s^{-1}$). Therefore, the as-

prepared β-$NaGdF_4$:Yb/Er@CaF_2 nanoparticles would be of great importance to wide application in clinical treatment and detection.

Acknowledgements

This work was financial supported in part by the National Science Foundation of China (Grants No. 21471043, 21101140) and the Key Project of Anhui Provincial Educational Department (JZ2014AJZR0113).

References and Notes

Department of Medical Materials and Rehabilitation Engineering, School of Medical Engineering, Hefei University of Technology, Hefei 230009, P. R. China. Fax: 0086 551 62901285; E-mail: yanglu@hfut.edu.cn (Y. Lu)*; shqian@hfut.edu.cn (Prof. H.S. Qian). B. Ding, K. Liu and F. Zhang contributed equally to this work.*

1 F. Caruso, *Adv. Mater.,* 2001, **13**, 11.

2 K. J. C. Van Bommel, A. Friggeri and S. Shinkai, *Angew. Chem. Int. Ed.,* 2003, **42**, 3027.

3 F. Zhang, G. B. Braun, Y. F. Shi, Y. C. Zhang, X. H. Sun, N. O. Reich, D. Zhao and G. Stucky, *J. Am. Chem. Soc.,* 2010, **132**, 2850.

4 F. Wang and X. G. Liu, *Acc. Chem. Res.,* 2014, **47**, 1378.

5 S. L. Gai, C. X. Li, P. P. Yang and J. Lin, *Chem. Rev.,* 2014, **114**, 2343.

6 L. D. Sun, Y. F. Wang and C. H. Yan, *Acc. Chem. Res.,* 2014, **47**, 1001.

7 R. A. Jalil and Y. Zhang, *Biomaterials,* 2008, **29**, 4122.

8 Fragioni, J. V. *Curr. Opin. Chem. Biol.,* 2003, **7**, 626.

9 Zhang, F.; Shi, Q. H.; Zhang, Y.; Shi, Y.; Ding, K.; Zhao, D.; Stucky, G. D. *Adv. Mater.,* 2011, **23**, 3775.

10 T. Yang, Y. Sun, Q. Liu, W. Feng, P. Yang, F. Li, *Biomaterials,* 2012, **33**, 3733.

11 Q. Dou, N. M. Idris and Y. Zhang, *Biomaterials,* 2013, **34***,* 1722.

12 C. Wang, L. Cheng, H. Xu and Z. Liu, *Biomaterials,* 2012, **33***,* 4872.

13 Y. Sun, X. Zhu, J. Peng and F. Li, *ACS Nano,* 2013, **7**, 11290.

14 Q. Liu, Y. Sun, T. Yang, W. Feng, C. Li and F. Li, *J. Am. Chem. Soc.,* 2011, **133***,* 17122.

15 S. S. Lucky, N. M. Idris, Z. Li, K. Huang, K. C. Soo and Y. Zhang, *ACS Nano,* 2015, **9**, 191.

16 H. S. Qian, H. C. Guo, P. C. Ho, R. Mahendran and Y. Zhang, *Small,* 2009, **5**, 2285.

17 G. B. Shan and G. P. Demopoulos, *Adv. Mater.,* 2010, **22**, 4373.

18 F. Li, C. Li, J. Liu, X. Liu, L. Zhao, T. Bai, Q. Yuan, X. Kong, Y. Han, Z. Shi and S. Feng, *Nanoscale,* 2013, **5**, 6950.

19 H. S. Qian and Y. Zhang, *Langmuir,* 2008, **24**, 12123.

20 C. Dong, A. Korinek,A.; B. Blasiak, B.Tomanek and F. C. J. M. van Veggel, *Chem. Mater.,* 2012, **24**, 1297.

21 X. Xie, N. Gao, R. Deng, Q. Sun, Q. H. Xu and X. Liu, *J. Am. Chem. Soc.,* 2013, **135**, 12608.

22 Q. Su, S. Han, X. Xie, H. Zhu, H. Chen, C. K. Chen, R. S. Liu, X. Chen, F. Wang, and X. Liu, *J. Am. Chem. Soc.*, 2012, **134**, 20849.

23 T. Grobner, *Nephrol. Dial. Transplant,* 2006, **21**, 1104.

24 L. Amuluru, W. High, K. M. Hiatt, J. Ranville, S. V. Shar, B. Malik and S. Swaminathan, *J. Am. Acad. Dermatol.,* 2009, **61**, 73.

25 G. Wang, Q. Peng and Y. Li, *J. Am. Chem. Soc.,* 2009, **131**, 14200.

26 G. Chen, J. Shen, T. Y. Ohulchanskyy, N. J. Patel, A. Kutikov, Z. Li, J. Song, R. K. Pandey, H. Ågren, P. N. Prasad, and G. Han, *ACS Nano,* 2012, **6**, 8280.

27 J. Shen, G. Chen, T. Y. Ohulchanskyy, S. J. Kesseli, S. Buchholz, Z. Li, P. N. Prasad, G. Han, *Small,* 2013, **9**, 3213.

28 C. Zhang, C. Li, C. Peng, R. Chai, S. Huang, D. Yang, Z. Cheng and J. Lin, *Chem-Eur. J.,* 2010, **16**, 5672.

29 X. Deng, Y. Dai, J. Liu, Y. Zhou, P. Ma, Z. Cheng, Y. Chen, K. Deng, X. Li and Z. Hou, Biomaterials, 2015, **50**, 154.

30 W. Zheng, S. Zhou, Z. Chen, P. Hu, Y. Liu, D. Tu, H. Zhu, R. Li, M. Huang and X. Chen, *Angew. Chem. Int. Ed.,* 2013, **52**, 6671.

31 X. F. Qiao, J. C. Zhou, J. W. Xiao, Y. F. Wang, L. D. Sun and C. H. Yan, *Nanoscale,* 2012, **4**, 4611.

32 C. Liu, Z. Gao, J. Zeng, Y. Hou, F. Fang, Y. Li, R. Qiao, L. Shen, H. Lei, W. Yang and M. Gao, *ACS Nano,* 2013, **7**, 7227.

33 S. J. Zeng, Z. Yi, W. Lu, C. Qian, H. Wang, L. Rao, T. Zeng, H. Liu, H. Liu, B. Fei and J. Hao, *Adv. Funct. Mater.*, 2014, **24**, 4051.

34 S. J. Zeng, M. K. Tsang, C. F. Chan, K. L. Wong and J. Hao, *Biomaterials*, 2012, **33**, 9232.

35 S. J. Zeng, H. Wang, W. Lu, Z. Yi, L. Rao, H. Liu and J. Hao, *Biomaterials*, 2014, **35**, 2934.

36 R. Naccache, F. Vetrone, V. Mahalingam, L. A. Cuccia and J. A. Capobianco, *Chem. Mater.,* 2009, **21**, 717.

37 L. Xiong, T.Yang, Y. Yang, C. Xu and F. Li, *Biomaterials,* 2010, **31**, 7078.

38 C. H. Liu, Z. Wang, H. X. Jia and Z. P. Li, *Chem. Commun.,* 2011, **47**, 4661.

39 S. J. Budijono, J. N. Shan, N. Yao, Y. Miura, T. Hoye, R. H. Austin, Y. G. Ju and R. K. Prud'homme,

Chem. Mater., 2010, **22**, 311.

40 J. F. Jin, Y. J. Gu, C. W. Y. Man, J. P. Cheng, Z. H. Xu, Y. Zhang, H. S. Wang, V. H. Y. Lee, S. H. Cheng and W. T. Wong, *ACS Nano,* 2011, **5**, 7838.

41 H. Q. Wang and T. Nann, *ACS Nano,* 2009, **3**, 3804-3808.

42 F. Wang, X. Fan, M. Wang and Y. Zhang, *Nanotechnology,* 2007, **18**, 025701.

43 J. Zhou, Y. Sun, X. Du, L. Xiong, H. Hu and F. Li, *Biomaterials,* 2010, **31**, 3287.

44 Z. Q. Li, Y. Zhang and S. Jiang, *Adv. Mater.,* 2008, **20**, 4765.

45 M. Bottrill, L. K. Nicholas and N. J. Long, *Chem. Soc. Rev*., 2006, **35**, 557.

46 Y. F. Wang, L. D. Sun, J. W. Xiao, W. Feng, J. C. Zhou, J. Shen and C. H. Yan, *Chem-Eur. J.,* 2012, **18**, 5558.

Graphic abstract

β-$NaGdF_4$:Yb,Er@CaF_2 core-shell nanoparticles: β-$NaGdF_4$:Yb/Er nanoparticles coated with ultrathin layer of CaF_2 are with enhanced upconversion fluorescence and chemical stability; which have been achieved via a sequential growth process.